Magnetic moments of lanthanide van der Waals dimers

Joseph McCann,[1] John L. Bohn,[1] and Lucie D. Augustovičová[2]
[1]*JILA, NIST, and Department of Physics, University of Colorado, Boulder, Colorado 80309-0440, USA*
[2]*Charles University, Faculty of Mathematics and Physics, Department of Chemical Physics and Optics, Ke Karlovu 3, CZ-12116 Prague 2, Czech Republic*

(Received 20 January 2021; accepted 2 April 2021; published 15 April 2021)

Loosely bound van der Waals dimers of lanthanide atoms, as might be obtained in ultracold atom experiments, are investigated. These molecules are known to exhibit a degree of quantum chaos due to the strong anisotropic mixing of their angular spin and rotation degrees of freedom. Within a model of these molecules, we identify different realms of this anisotropic mixing, depending on whether the spin, the rotation, or both are significantly mixed by the anisotropy. These realms are in turn generally correlated with the resulting magnetic moments of the states.

DOI: 10.1103/PhysRevA.103.042812

I. INTRODUCTION: MOLECULAR COMPLEXITY

The harmony and quietude of ultracold atoms were shattered in 2014 with the discovery that collisions of erbium atoms at 300 nK exhibited the telltale signs of quantum chaos [1], followed by similar observations in dysprosium [2,3] and thulium [4], as well as dysprosium-erbium mixtures [5]. Magnetic field scans revealed not only an unprecedented host of Fano-Feshbach resonances, but also that the magnetic field locations of these resonances appeared to be distributed according to the predictions of random matrix theory, a finding suggestive of quantum chaos. The observations attest to the unexpected complexity of weakly bound lanthanide dimer molecules within several gigahertz of their dissociation threshold.

This observation is a challenging one to interpret within the paradigms of quantum chaos. For one thing, it is not completely clear that the resolution in the experiments was capable of detecting all the resonances. Disregarding the very narrow ones may bias the spectrum toward revealing less chaos than it truly possesses [6]. Further, while a common statistical analysis tool—the Brody function that characterizes the distribution of nearest-neighbor spacings in the spectrum—showed evidence of chaos, its appropriateness has been called into question. The claim was made that perhaps the data were better fit by a semi-Poisson distribution, revealing the system to be quasi-integrable [7]. Another complication arises with regard to the unusual nature of the experiments. Typically, quantum chaos studies the spectrum and eigenfunctions of a given Hamiltonian. By contrast, the ultracold experiments determine a spectrum of magnetic field values at which Fano-Feshbach resonances occur. Thus the spectrum identifies a single, zero-energy eigenstate from each of an ensemble of different Hamiltonians, one for each magnetic field. It is not immediately obvious how to view nearest-neighbor spacings in such a circumstance [8].

These issues were clarified by a combination of experiment and theory that looked at the Fano-Feshbach spectra in both Er and Dy, comparing them to the results of large-scale scattering computations [3]. It was concluded that the observed Brody parameters corresponding to the magnetic field spectra could indeed be accounted for. This required appreciating that, not only were the atoms complex, with many internal spin states, but also that these states were strongly coupled by anisotropic interactions during their collision [9]. The observation of chaos was therefore one of the fruits of a decade-long process of cooling and trapping strongly anisotropic atoms by such techniques as buffer-gas [10,11] or laser cooling [12–16].

More significantly, the calculation of Ref. [3] revealed that the degree to which the energy spectrum is chaotic is contingent on the value of the magnetic field at which the spectrum is generated. Further evidence of order amid the chaos appears in measurements of molecular bound states by magnetic field modulation spectroscopy near broad Fano-Feshbach resonances [17,18]. These measurements and subsequent analysis identify these bound states as being of essentially single-channel, *s*-wave character, unencumbered by significant coupling to other angular momentum states.

Numerical models of the spectrum can, of course, reveal information about the molecules that the experiment is not yet privy to. Thus Ref. [19] applied more sophisticated statistical tests, including a family of information-theoretic entropies, to the numerical spectrum from Ref. [3], looking at the energy range 0.5 GHz below threshold. Unlike the experiments, this calculation was able to evaluate a significant region of the energy spectrum at any desired magnetic field, along with the energy eigenstates. A main conclusion is that the spectrum exhibits "multifractal" behavior, quantifying the degree to which the spectrum appears chaotic. Moreover, various measures of quantum chaos were seen to increase as the magnetic field grew larger and channel mixing increased.

Generally, analysis in terms of entropies is useful in locating complex systems along the complexity scale. For truly random systems, whose spectra are well described statistically in random matrix theory, this theory provides upper limits to the values of entropies [20]. Many physical systems fall short

of this upper limit and have submaximal entropies, suggesting that some order remains [20,21]; this is the case for the model of Ref. [19]. A consequence of the previous analyses is therefore that lanthanide dimers just below their dissociation threshold are complicated, yes, but they are not thoroughly chaotic. There may be something orderly about them, at least in some eigenstates, that can be expressed in terms of the familiar ingredients of molecular physics, namely, vibrations, rotations, and spins, and their quantum numbers. In favorable cases, this would entail identifying good quantum numbers, or nearly good quantum numbers, so that an appropriate Hund's case might be identified. On the other hand, it may be the case that in some states this is not possible and the objects of quantum chaos theory become the appropriate tools for describing the states, or at least specific ensembles of states.

In this spirit, this article will examine weakly bound van der Waals Dy_2 dimers and seek to understand which, if any, quantum numbers remain good, and under what circumstances. To give a specific context, we associate this search to concrete observable quantities of the molecular states, namely, their magnetic moments. These weakly bound dimers can be created in the laboratory, say by magnetoassociation, and their magnetic dipole moments can be measured [22]. They may also perhaps be accessible by microwave spectroscopy. In any event, we pursue statistical aspects of a distribution of magnetic moments, which in general are uncorrelated to the energies of the states, but which provide insight into the composition of molecular wave functions.

In the current article we focus for simplicity on molecules in zero magnetic field, where the total angular momentum is conserved. We find that the states with fairly well-defined angular momentum quantum numbers tend to be those that are stretched, with near-maximal values of certain angular momenta. As a consequence, the more orderly versus more chaotic states can be distinguished, on average, by the values of their magnetic moments.

II. SCOPE OF THE PAPER

We contemplate a diatomic molecule composed of two identical lanthanide atoms, such as Dy, Er, Tm, etc. In practice, for the calculations below we will use Dy and explicitly consider bosonic isotopes with zero nuclear spin. Each of the atoms has spin $\mathbf{j}$ and magnetic moment $\boldsymbol{\mu} = -g\mu_B\mathbf{j}$, where $\mu_B = e\hbar/2m_ec$ is the Bohr magneton, expressed in cgs units; and g is the atom's g factor, here defined as a positive number. Thus in an applied magnetic field that defines the laboratory z axis, the energies of the atom depend on the field as $g\mu_B Bm$, for state $|jm\rangle$. This expression for energy shift is accurate for fields small enough such that j remains a good quantum number.

When two lanthanide atoms are combined into a van der Waals dimer, the resulting molecule is a composite object with total angular momentum $\mathbf{J} = \mathbf{j}_1 + \mathbf{j}_2 + \mathbf{L}$, where $\mathbf{j}_i$ is the spin of the ith atom and $\mathbf{L}$ is the orbital angular momentum of the atoms about their center of mass. We use $\mathbf{L}$ for this quantity to draw the analogy with the partial wave angular momentum in ultracold collisions of the atoms. Since the atoms are electrically neutral, the orbital motion does not contribute to the magnetic moment of the molecule, whose moment is therefore $\boldsymbol{\mu} = -g\mathbf{j}_1 - g\mathbf{j}_2$. The extreme values of the moment occur when $m_1 = m_2 = \pm j$, whereby the molecular magnetic moment must lie between $\pm g\mu_B(2j)$. For Dy, with $j = 8$ and $g = 1.2416$, these bounds are $\pm 19.9\mu_B$. Various states of the molecule will have magnetic moments between these two limits, depending on the details of how the state is constructed. The moment is therefore a probe of how the separate angular momenta work together in the molecule.

The number of possible energy eigenstates of these molecules is vast. To lend focus to the current investigation, we strongly constrain its scope to a set of molecular states close to experimental reality. Specifically, we will consider a pair of spin-stretched Dy atoms initially in their lowest-energy state $|jm\rangle = |8 - 8\rangle$. A small field may be applied to remove the degeneracy of the states. These atoms are assumed to collide via an s-wave collision with $L = 0$; hence the total angular momentum of the atom pair is $|JM\rangle = |16 - 16\rangle$, and this angular momentum is considered to be conserved in sufficiently small magnetic field. It is conceivable, if not necessarily easy, to perform a microwave spectroscopy experiment that associates the free atoms into weakly bound states of the Dy_2 dimer. Measurements of the energy E_α at two distinct, small magnetic fields allow the determination of the magnetic moment of state $|\alpha\rangle$ via $\mu_\alpha = \Delta E_\alpha/\Delta B$. The statistical distribution of the moments so defined is the subject of our inquiry.

III. MODEL

Given the complexity of the lanthanide van der Waals dimers, a complete and accurate *ab initio* theory of their structure remains challenging. Nevertheless, guided by previous models, some of the salient features of the dimers are apparent. The predominant features of the interatomic interactions at large interatomic separation consist of the magnetic dipole-dipole interaction and the anisotropic van der Waals interaction, the latter of which is believed to be primarily responsible for the channel mixing that generates some degree of chaos in the molecular spectrum [3]. We will therefore include these interactions in some detail. By contrast, our representation of the Born-Oppenheimer potentials will be somewhat more schematic, as they are less important to the present analysis.

A. Basis sets and Hamiltonian

To attain the total angular momentum J requires coupling the spins of the two atoms to their relative orbital angular momentum. Formally, this can be done in either the laboratory frame or else in the body frame of the molecule. In either case, we use as an intermediate the total spin angular momentum of the two atoms, $\mathbf{j}_{12} = \mathbf{j}_1 + \mathbf{j}_2$. We contemplate two basis sets for the molecule, resembling the Hund's cases (a) and (b), familiar from the theory of diatomic molecules.

For brevity, we suppress the notation j_1, j_2 of the individual spins as being understood. Then in the body frame, the basis set is written

$$|j_{12}\bar{\Omega}; JM\rangle = \frac{1}{\sqrt{2(1+\delta_{\bar{\Omega}0})}}[|j_{12}\bar{\Omega}\rangle|\bar{\Omega}JM\rangle + (-1)^{J-j_{12}}|j_{12} -\bar{\Omega}\rangle|-\bar{\Omega}JM\rangle], \quad (1)$$

where

$$|j_{12}\Omega\rangle = \sum_{\omega_1\omega_2} |j_1\omega_1\rangle|j_2\omega_2\rangle\langle j_1\omega_1 j_2\omega_2|j_{12}\Omega\rangle, \quad (2)$$

$$|\Omega JM\rangle = \sqrt{\frac{2J+1}{8\pi^2}} D^{J*}_{M\Omega}(\phi,\theta,\gamma), \quad (3)$$

with ω_i the projection of spin $\mathbf{j}_i$ on the interatomic axis. The Wigner rotation matrix D is a function of the Euler angles (ϕ,θ,γ) that relate the body frame to the laboratory frame. The spins of the atoms are quantized along the body-frame axis, identifying this basis set as analogous to Hund's case (a). Here $\bar{\Omega} = |\Omega|$ is intrinsically non-negative and takes the values $\bar{\Omega} = 0, 1, \ldots, \min(j_{12}, J)$. For the example considered in this paper, only even values of j_{12} are allowed; thus $\bar{\Omega} = 0$ is possible only when J is even.

The alternative useful basis set is the laboratory-frame basis, given by

$$|[j_{12}L]JM\rangle = \sum_{m_{12}M_L} |j_{12}m_{12}\rangle|LM_L\rangle\langle j_{12}m_{12}LM_L|JM\rangle, \quad (4)$$

where in the laboratory frame,

$$|j_{12}m_{12}\rangle = \sum_{m_1m_2} |j_1m_1\rangle|j_2m_2\rangle\langle j_1m_1j_2m_2|j_{12}m_{12}\rangle, \quad (5)$$

and the rotation of the molecule is described by the orbital angular momentum wave functions

$$|LM_L\rangle = Y_{LM_L}(\theta,\phi) = \sqrt{\frac{2L+1}{4\pi}} C_{LM_L}(\theta,\phi), \quad (6)$$

where C_{LM_L} is a reduced spherical harmonic. This basis is already symmetric under exchange of the identical bosons, provided that $j_{12} + L$ is even. Quantization of the atomic spins in the laboratory frame identifies this basis set as analogous to Hund's case (b).

For the examples considered in this paper, linked to a presumed initial state defined by s-wave scattering with $L = 0$, our identical bosons can only access states with even values of j_{12}, that is, gerade states of the interatomic potential energy surfaces. We will impose this restriction on the results below.

The Hamiltonian can be written as a sum of contributions,

$$H = T + H_{\rm BO} + H_{\rm dd} + H_{\rm ad} + H_{\rm B}, \quad (7)$$

which are the following, in order: kinetic energy, the Born-Oppenheimer potentials responsible primarily for short-range interactions, the long-range dipole-dipole interaction, the long-range anisotropic dispersion interaction, and the magnetic field Hamiltonian. The appropriate theoretical machinery for describing matrix elements of the Hamiltonian is in terms of tensor operators, whose theory is developed in detail elsewhere [23–25]. The Hamiltonian is characterized by an R-dependent effective potential energy $V(R)$, whose matrix elements are given in the Appendix.

B. Vibration

The remaining degree of freedom, in R, defines the vibrational motion in the potential energy V. Each basis set above defines a particular realization of a set of R-dependent diabatic channels, which would be suitable for scattering calculations. We denote for brevity this set of quantum numbers by the collective ket $|d\rangle$, which stands for either the body-frame channel basis (1) or else the laboratory-frame channel basis (4).

In the usual way, we write the total wave function in the form $\Psi(R,\sigma) = R^{-1} f(R,\sigma)$, where σ denotes all coordinates other than the interatomic spacing R. The wave function $R\Psi$ is acted upon by the Hamiltonian

$$H = -\frac{\hbar^2}{2m_r}\frac{d^2}{dR^2} + V_{\rm d}(R) + V_{\rm od}(R), \quad (8)$$

where $V_{\rm d}$ is a set of diabatic potential curves, consisting of the diagonal matrix elements of $V(R)$ as expressed in this basis, while $V_{\rm od}$ contains all of the off-diagonal matrix elements.

Each potential $V_{\rm d}$ possesses a set of vibrational bound states, given by

$$-\frac{\hbar^2}{2m_r}\frac{d^2 f_{d,v_d}}{dR^2} + V_{\rm d} f_{d,v_d} = E_{d,v_d} f_{d,v_d}. \quad (9)$$

The set of states

$$|i\rangle \equiv |d, v_d\rangle = |d\rangle f_{d,v_d} \quad (10)$$

therefore constitutes an approximate set of molecular states for our lanthanide diatom. These states represent the molecular states as accurately as possible, while still retaining rigorously good values of the angular momentum quantum numbers d of the body or laboratory frame, and a well-defined vibrational quantum number. We will refer to these as the molecular basis states. If they are minimally mixed, then their quantum numbers are still a valid way to express the states of the molecule; if they are strongly mixed, then they serve to identify what, exactly, is being mixed on the way toward making the molecule chaotic.

The wave function can then be expanded in this basis:

$$f = \sum_{dv_d} c_{dv_d} |dv_d\rangle. \quad (11)$$

Solving the Schrödinger equation amounts to diagonalizing the Hamiltonian $\mathcal{H}$ in the extended basis $|dv_d\rangle$. The diagonal elements of this matrix are

$$\langle dv_d|\mathcal{H}|dv_d\rangle = E_{dv_d}, \quad (12)$$

while those matrix elements explicitly off-diagonal in d are given by

$$\langle dv_d|\mathcal{H}|d'v'_d\rangle = \int dR f_{dv_d}(R)\langle d|V_{\rm od}|d'\rangle f_{d'v'_d}(R), \quad (13)$$

and matrix elements of $V_{\rm od}$ can be computed term by term, knowing the explicit form of the various terms as given above.

We obtain the molecular spectrum by diagonalizing the Hamiltonian matrix in these terms. The vibrational states are computed in each diabatic channel by a Fourier grid Hamiltonian method [26], subject to box boundary conditions at the radius $R_2 = 400a_0$. This truncation may alter those states within about $\hbar^2/(2m_rR_2^2) \approx 0.1$ MHz, which represents a negligible part of the spectrum we study. In order to achieve convergence of the final spectrum, we must include states in the quasicontinuum of this box.

C. Magnetic moments of the basis states: *g* factors

The basis states defined in the previous section afford the simplest model of the magnetic moment distribution of the molecules. In the absence of channel coupling, and in the limit of zero magnetic field, all the quantum numbers remain good. In this case the magnetic moments of the states may be described by analytical formulas.

We can write the magnetic moments in terms of g factors as

$$\mu_i^{\text{basis}} = g(i)\mu_B M. \tag{14}$$

Expressions for the g factors can then be derived by evaluating diagonal matrix elements of the magnetic Hamiltonian. In the body frame these are

$$g(j_{12}, \bar{\Omega}, J) = \frac{\bar{\Omega}^2}{J(J+1)}, \tag{15}$$

while in the laboratory frame they are

$$g(j_{12}, L, J) = \frac{1}{2}\left[1 + \frac{j_{12}(j_{12}+1) - L(L+1)}{J(J+1)}\right]. \tag{16}$$

These are, of course, familiar expressions in molecular physics [27].

One can then define a statistical distribution of magnetic moments for either of these forms by simply giving the occurrence of each possible quantum number equal weight. The statistical distribution of the moments in the body frame would count each value of j_{12} from 0 to $2j$, counting only even values for the gerade states we consider here, and values of $\bar{\Omega}$ from j_{12} up to $2j$. For Dy with $j = 8$, this amounts to 81 possibilities. Counting each such possibility equally would give a distribution with the mean and standard deviation for the magnetic moments:

$$\bar{\mu}_{body} = g\mu_B M \frac{2j+3}{12(j+1)}$$
$$\sigma(\mu)_{body} = g\mu_B |M| \sqrt{\frac{(28j^2+24j-9)(j+2)(2j+3)}{720j^2(2j+1)}}. \tag{17}$$

Likewise, in the laboratory frame the quantum number for gerade states will run even values of j_{12} from 0 to $2j$, while L runs, also in even values, from $|J - j_{12}|$ to $J + j_{12}$, where $J = 2j$ in the examples considered here. Counting each possibility equally gives, for the laboratory frame,

$$\bar{\mu}_{lab} = g\mu_B M \frac{2j+3}{12(j+1)}$$
$$\sigma(\mu)_{lab} = g\mu_B |M| \sqrt{\frac{264j^3+548j^2+286j-3}{720j^2(2j+1)}}. \tag{18}$$

The mean value of the magnetic moment is the same in either basis [28], but the standard deviations are quite different.

For the $j = 8$ Dy atom in our examples, and in the state where $J = 16$, $M = -16$, we find that, in the body frame, the mean of the magnetic moment distribution is $-3.49\mu_B$, and the standard deviation of the distribution is $4.35\mu_B$. By contrast, in the lab frame the mean of the distribution is the same, but its standard deviation is $9.32\mu_B$, significantly larger. Deviations of the distribution of the true magnetic moments from these values can be viewed as evidence of the mixing of basis states in the true energy eigenstates. It will be recalled that these results are for the particular case of total angular momentum equal to twice the atomic angular momentum, $J = 2j$. Other manifolds of states will have analogous statistical distributions, of course.

D. Magnetic moments of the fully coupled molecule

Realistically, the distribution of magnetic moments can be strongly modified by channel couplings in the physical model of the molecule. Having the matrix representation in hand, we can compute the magnetic moments in the model. Generically, at any value of the magnetic field B, suppose the Hamiltonian is written

$$H = H_{\text{mol}} + \mathcal{M}B, \tag{19}$$

where H_{mol} is the complete molecular Hamiltonian in zero field and $\mathcal{M}$ is a magnetic moment matrix with $\mathcal{M}B = H_{\text{B}}$. Suppose we desire the magnetic moments at a magnetic field B. Then we contemplate a perturbation of the field ΔB and write the Hamiltonian

$$H = H_{\text{mol}} + \mathcal{M}B + \mathcal{M}\Delta B. \tag{20}$$

Let U be the matrix whose columns are the eigenvectors of $H_{\text{mol}} + \mathcal{M}B$, so that the energies of the molecule at field B are the diagonal elements of

$$\text{diag}(E_\alpha(B)) = U^T(H_{\text{mol}} + \mathcal{M}B)U. \tag{21}$$

Casting the full Hamiltonian in this basis, we get

$$U^T H U = \text{diag}E_\alpha(B) + U^T \mathcal{M} U \Delta B, \tag{22}$$

whereby, in the perturbative limit, the magnetic moments of the states are given by

$$\mu_\alpha \approx \frac{\Delta E_\alpha}{\Delta B} = (U^T \mathcal{M} U)_{\alpha\alpha}. \tag{23}$$

This expression is used to calculate the magnetic moments, in the zero-field limit, in the examples below.

IV. RESULTS

A. Comparison of the basis states

Given the two standard basis sets, in the body and laboratory frames the first question is to inquire which, if either, is a better representation of the full energy eigenstates of the molecule. To this end, we deploy the participation number, defined as follows. Any eigenstate $|\alpha\rangle$ of the Hamiltonian is expressed in a basis $|i\rangle$ by $|\alpha\rangle = \sum_i |i\rangle\langle i|\alpha\rangle$. Given this expansion, the participation number is given by [21]

$$D(\alpha) = \left(\sum_i |\langle i|\alpha\rangle|^4\right)^{-1}. \tag{24}$$

This and related entropies, such as the Shannon entropy, serve to measure the deviation of the energy eigenstates $|\alpha\rangle$ from the basis states $|i\rangle$ from which they are forged. For example, if the energy eigenstate is already uniquely identified by the basis

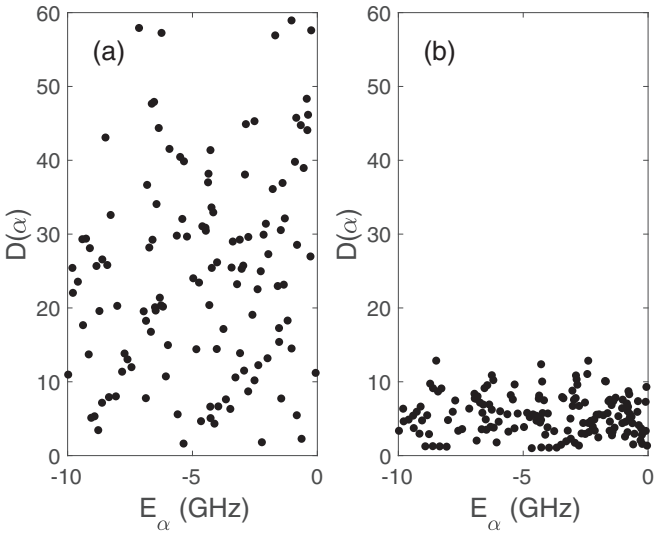

FIG. 1. Participation number $D(\alpha)$ of each energy eigenstate $|\alpha\rangle$ in the model vs energy E_α of the state. $D(\alpha)$ is computed with respect to the coupled body frame $|j_{12}\bar{\Omega};JM\rangle$ in (a), and with respect to the coupled laboratory-frame basis $|[j_{12}L]JM\rangle$ in (b).

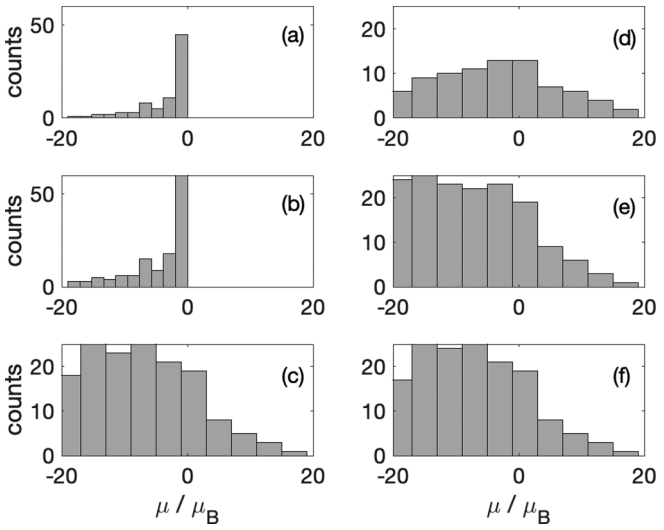

FIG. 2. Distributions of magnetic moments in the model Dy_2 molecules at various levels of approximation. Left panels: body frame. Right panels: laboratory frame. Top row: statistical moments. Middle row: basis moments (see text). Bottom row: the final, physical moments, which are, of course, the same in both calculations.

state $|i\rangle$, i.e., if $|\langle i|\alpha\rangle| = 1$, then $D(\alpha) = 1$; only a single basis state participates. Alternatively, if n states equally participate and $|\langle i|\alpha\rangle| = 1/\sqrt{n}$ for each of them, then $D(\alpha) = n$ counts them. In this paper we prefer the participation number to the Shannon entropy because of the significance of the value $D(\alpha) = 1$ in identifying states of good quantum number.

We have calculated an exemplary spectrum, using the model described in the previous section, in terms of both the body and the laboratory basis set, assuming zero magnetic field. These are converged so as to give the same spectrum for both calculations. In Fig. 1 we plot the participation number of the states versus the energy of the state, for the part of the spectrum lying 10 GHz below the dissociation threshold. This is shown for both the coupled body-frame basis set (a) and the laboratory-frame basis set (b).

It is immediately clear that $D(\alpha)$ is greater for the body-frame basis than for the laboratory-frame basis, thus the latter is more likely a reasonable description of the states. This comparison affords complementary perspectives on the origin of chaos. In the body frame, potential interactions such as the model Born-Oppenheimer curves, the dipole-dipole interaction, and the anisotropic van der Waals interaction are diagonal in the quantum number $\bar{\Omega}$, which ought to make this quantum number appropriate for the description of the states. However, near threshold the molecule, rotating with high angular momentum, is subject to strong Coriolis coupling, which thoroughly mixes the different $\bar{\Omega}$ states. From this point of view, chaos arises from couplings due to kinetic energy,

From the other perspective, in the laboratory frame the kinetic energy is already diagonal in the rotational quantum number L. The states of different L are mixed by the potential interaction terms, primarily the anisotropic van der Waals interaction. This is a less significant mixing of the basis states, as evidenced by the smaller participation number. We may therefore try to identify the magnetic moments in terms of the laboratory-frame g factors in Eq. (16).

B. Magnetic moments in the coupled states

The superiority of the laboratory frame over the body frame is shown in more detail by considering the distribution of magnetic moments. To see this, we present in Fig. 2 various distributions of magnetic moments for the $J = 16$, $M = -16$ state of Dy_2, computed at various levels of approximation. In the first column, panels (a), (b), (c), we have results calculated in the body-frame basis. In the second column, panels (d), (e), (f) are results from the laboratory-frame calculation. In each case, the first row represents the statistical distribution of magnetic moments, as given by Eqs. (15) and (16), weighting the occurrence of each possible quantum number equally. The middle row describes the distribution of "basis moments," those that belong to the rovibrational states defined in (10). Finally, the third row of Fig. 2 includes the physical distribution of magnetic moments, including all channel couplings. It is, of course, the same in panels (c) and (f), as the physical result does not depend on the basis used to calculate it. Recall that the moments for states of Dy_2 with $J = 16$ should lie between $\pm 19.9\mu_B$. This entire range is represented in the actual moments, although they are biased toward negative values for the $M = -16$ state considered.

Panels (a) and (d) represent the statistical moment distributions, which have the means and standard deviations given by Eqs. (27) and (28), respectively. The body-frame moments in (a) are heavily weighted near zero, since the value of $\bar{\Omega} = 0$ occurs many times in this set of quantum numbers, once for each value of j_{12}. The distribution in (a) is far from the physical distribution in (c) since, as noted above, states with different $\bar{\Omega}$ get strongly mixed by Coriolis forces in the real molecule. By contrast, the statistical distribution of magnetic moments in the laboratory frame, (d), already resembles the final distribution in (f). The laboratory-frame g factors are already a good first guess at the molecular moments but differ in details.

TABLE I. Mean, $\bar{\mu}$, and standard deviation, $\sigma(\mu)$, for the distributions of magnetic moments shown in Fig. 2.

	Body frame	Laboratory frame
$\bar{\mu}$, statistical	−3.49	−3.49
$\sigma(\mu)$, statistical	4.35	9.32
$\bar{\mu}$, basis	−4.18	−7.37
$\sigma(\mu)$, basis	4.88	8.64
$\bar{\mu}$, full	−7.23	−7.23
$\sigma(\mu)$, full	8.28	8.28

The second row adds a little bit to the physics of the molecules by incorporating the vibrational structure while still assuming rigorously good quantum numbers in either basis. Because vibrational motion in the diabatic potential energy surfaces is considered, the energies shift somewhat and so do the magnetic moments, from the statistical distribution. These shifts do not affect the body-frame moments much, i.e., panels (a) and (b) are similar.

In the laboratory frame, the main difference between the statistical moments and the basis moments is that the basis moments in panel (e) tend to favor lower values than the statistical moments in panel (d). These basis moments include vibrational motion in R and hence are influenced by (among other things) the centrifugal potential $\hbar^2 L(L+1)/2m_r R^2$ in each channel. For larger values of L, the distance between the inner and outer turning points of the diabatic potential V_d are closer together, contributing to higher radial kinetic energy. As a consequence, the vibrational spacing is larger and there are fewer states of high L to be found in the energy interval considered. According to (16), these high-L states tend to correspond to lower g factors, or to higher magnetic moments for the $M = -16$ states we consider here [see (14)]. Hence, states of higher L are less common in (e) than in (d), with the consequence that there are fewer positive magnetic moments.

The physical distributions of magnetic moments, including the full channel coupling, are given in panels (c) and (f) for this model. This calculation includes all the additional off-diagonal coupling between the rovibrational states used in panels (b) and (e). These couplings influence the body-frame moments dramatically and the laboratory-frame results less so. In either case, however, the distributions in the fully coupled calculations must be the same, as seen by the means and standard deviations of the moments presented in Table I. Taken together, we conclude that in the laboratory-frame basis, states with good values of the quantum numbers j_{12} and L, distributed as in Fig. 2(e), already very nearly comprise the correct distribution.

C. Reduced density matrices

The laboratory frame is unambiguously the better set of quantum numbers to describe the molecules and their magnetic moments. The basis is not perfect, however; mixing of these states really does occur. A further look into the structure of the molecules would investigate which degrees of freedom are most strongly mixed and which are weakest, i.e., which of the several degrees of freedom possesses the best quantum numbers.

To quantify the goodness of a given quantum number, we employ additional concepts from information theory. In the first step we cast the problem in the language of density matrices. In terms of the expansion coefficients $\langle\alpha|i\rangle$ of the state $|\alpha\rangle$ in the basis $|i\rangle$, we construct a diagonal density matrix with elements

$$\rho_{ii'}(\alpha) = |\langle\alpha|i\rangle|^2 \delta_{ii'}. \tag{25}$$

This has the essential property that a density matrix should possess, namely, $\mathrm{Tr}(\rho) = 1$. This ρ would be analogous to a pure state if it had only a single nonzero element, whereby we would have $\mathrm{Tr}(\rho^2) = 1$. More generally, $\mathrm{Tr}(\rho^2)$ falls short of unity, and the occurrence of multiple basis states in the eigenstate corresponds to the density matrix representing a mixed, as opposed to a pure, state. This is indeed how one makes the intellectual transition to the entropy, given as

$$S(\alpha) = -\mathrm{Tr}(\rho \ln \rho). \tag{26}$$

Casting the state in terms of this apparent density matrix allows us to extract reduced density matrices for the different degrees of freedom. For example, the laboratory basis is indexed by its quantum numbers $|i\rangle = |j_{12}, L, v\rangle$ (assuming fixed J, M). Then we can extract the reduced density matrix in, say, the j_{12} quantum number via

$$\bar{\rho}_{j_{12}}(\alpha) = \sum_{L,v} \rho_{j_{12},L,v;j_{12},L,v}(\alpha) = \sum_{L,v} |\langle\alpha|j_{12}, L, v\rangle|^2. \tag{27}$$

Treating j_{12} as the only remaining degree of freedom, we can assign a reduced entropy to the state, or in our case, a reduced participation number, given by

$$\bar{D}_{j_{12}}(\alpha) = \left(\sum_{j_{12}} \bar{\rho}^2_{j_{12}}(\alpha)\right)^{-1} = \left(\sum_{j_{12}} \left[\sum_{L,v} |\langle\alpha|j_{12}, L, v\rangle|^2\right]^2\right)^{-1}. \tag{28}$$

Low values of $\bar{D}_{j_{12}}(\alpha)$ correspond to states where j_{12} is a nearly good quantum number in state $|\alpha\rangle$, regardless of whether the other quantum numbers are good or not. The analogous reduced density matrices and participation numbers $\bar{D}_L(\alpha)$, $\bar{D}_v(\alpha)$ for the other degrees of freedom can be defined analogously.

The participation number is shown for the three relevant quantum numbers of the laboratory-frame basis set in Fig. 3, for the same data as in Fig. 2. Panel (a) shows $\bar{D}_v(\alpha)$ for the vibrational quantum number of the atoms. It is almost uniformly equal to unity, except perhaps very near the dissociation threshold. We conclude that vibrational states are only weakly mixed, in this basis, upon the introduction of potential coupling between the channels.

Figure 3(b) shows the reduced participation number $\bar{D}_L(\alpha)$ for the rotation of the atoms about their center of mass. We note that for the current model with $J = 16$, L can take all the even values up to 32, or seventeen values in all, whereby $\bar{D}_L(\alpha)$ could conceivably be as large as seventeen for thorough mixing of all the L states. While $\bar{D}_L(\alpha)$ occasionally approaches this limit for some states, nevertheless it is nearly equal to unity for a large fraction of the states in this energy

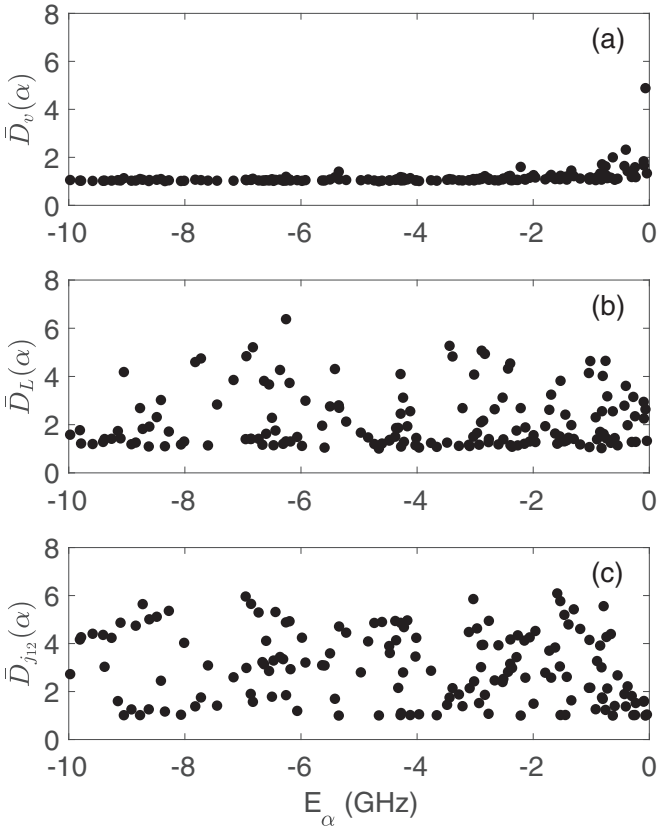

FIG. 3. Reduced participation numbers for the three relevant quantum numbers in the laboratory-frame basis set for the $J = 16$, $M = -16$ states of Dy_2 near threshold.

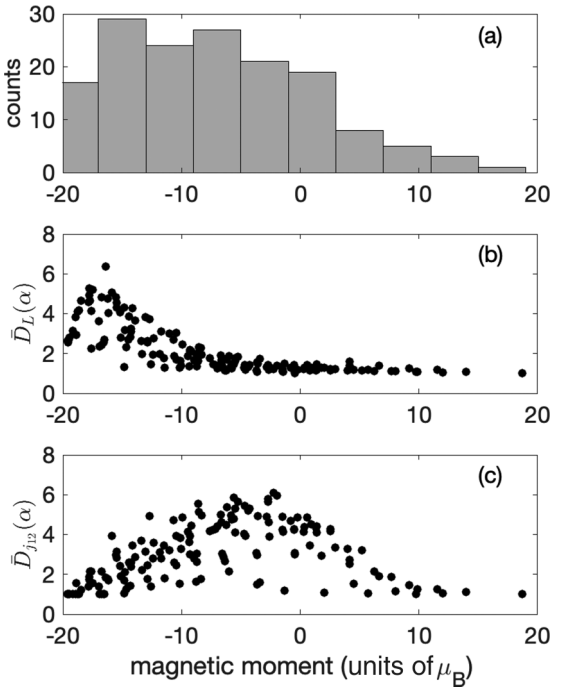

FIG. 4. Reduced participation numbers for j_{12} and L, for the $J = 16$, $M = -16$ states of Dy_2 near threshold. These quantities are plotted vs the magnetic moment of the states, also counted in the histogram in panel (a).

range. This is consistent with the tale told above, that L in the laboratory-frame basis set is appropriate for describing the states. The fact that $\bar{D}_L(\alpha)$ is often close to 1 is evidence that the states are not thoroughly chaotic, as they do not strongly mix the different L states. It is significant, however, that some states apparently do mix various L states.

The real mixing of basis states occurs for the total spin angular momentum j_{12}, whose reduced participation number $\bar{D}_{j_{12}}(\alpha)$ is shown in Fig. 3(c). For the Dy_2 model considered, j_{12} can take even values form 0 to $2j = 16$, or nine values in all, setting an upper limit to the value of $\bar{D}_{j_{12}}(\alpha)$. This limit is never quite achieved for these states, but there is certainly more scatter in the values of $\bar{D}_{j_{12}}(\alpha)$ than there is for $\bar{D}_L(\alpha)$. It appears, therefore, that the greatest channel mixing that contributes to the chaotic behavior of the molecule lies in the mixing of the atomic spins. Nevertheless, even in this case there exist states with good values of j_{12}, where $\bar{D}_{j_{12}}(\alpha) \approx 1$.

D. Regularities of the eigenstates

It is instructive to plot the participation numbers for the angular momentum degrees of freedom in an alternative way, as in Fig. 4. Panels (b) and (c) show, respectively, the reduced participation numbers $\bar{D}_L(\alpha)$ and $\bar{D}_{j_{12}}(\alpha)$ for each eigenstate as a function of the magnetic moment of that state. As a reference, panel (a) repeats the histogram of the magnetic moment distribution from Fig. 2.

In this figure a semblance of order emerges in the correlation between participation number and magnetic moment. Namely, as shown in Fig. 4(b), states with the highest magnetic moments, down at least to the mean $\bar{\mu} = -7.23\mu_B$, have low participation number $\bar{D}_L(\alpha)$—they are states where L is a good quantum number. The states with lower magnetic moments are more often mixtures of states with different L values. Likewise, a clear trend emerges in Fig. 4(c). States with extreme values of μ, either high near $20\mu_B$ or low near $-20\mu_B$, tend to contain few j_{12} values. By contrast, states with intermediate values, around the mean $\bar{\mu}$, mix together several j_{12} states.

These results are qualitatively explained using semiclassical angular momentum coupling diagrams [29], as in Fig. 5. In this diagram the $\hat{z}$ direction of the laboratory axis points upward, whereby the angular momentum state $J = 16$, $M = -16$ is represented by the arrows pointing straight down in all figures. (In the semiclassical representation this vector would make a small angle $\cos^{-1}[16/\sqrt{(16 \times 17)}]$ with respect to the axis, which we here disregard for clarity of the diagram.) In the laboratory frame, this large angular momentum is described as the sum of the rotation $\mathbf{L}$ and the total spin $\mathbf{j}_{12}$, indicated in the figure for positive, negative, and near-zero values of magnetic moment in (a), (b), and (c), respectively. In each case, these angular momenta determine the relative orientation of the atoms (gray circles) and indicate the kind of orientation of the spins (thick red arrows). In this picture the more upward the spins are allowed to point, the greater their magnetic moment.

Consider first the case of large positive magnetic moment Fig. 5(a). To achieve this result, the spin angular momentum is

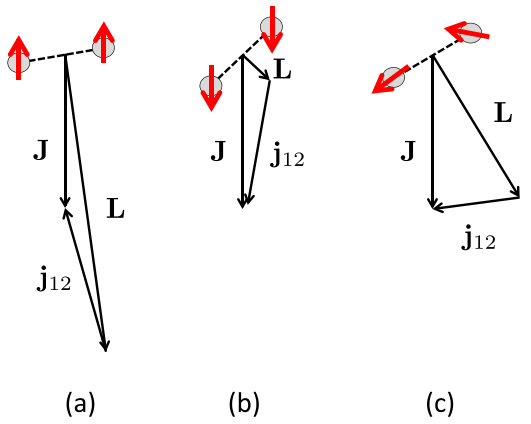

FIG. 5. Schematic, classical representation of the angular momentum coupling of the molecule. Gray circles represent the atoms, and thick red arrows are their magnetic moments. Shown are the cases: (a) large values of L, (b) small values of L, and (c) intermediate values of L.

near its maximum value $j_{12} = 16$. There are few comparable j_{12} states available to mix together, so in this limit j_{12} remains a reasonably good quantum number. In order to attain the total angular momentum $\mathbf{J}$, the rotational angular momentum must be near its maximum value $L = 32$ but pointing in the other direction. Consequently, it is not mixed with many other L values either, and both j_{12} and L remain good quantum numbers for large magnetic moment.

Next, consider a large negative magnetic moment, Fig. 5(b). To achieve this result, j_{12} must again be near its maximum magnitude but with a classical vector pointing downward, so j_{12} remains a nearly good quantum number. In this case, however, L must be small in magnitude and can take various small values while requiring only small changes in $\mathbf{j}_{12}$ to add to the total J. Even small values of $\mathbf{L}$ can represent states where the molecular orientation makes a significant angle with respect to the spin axis, as indicated in the figure. Therefore, in the presence of the kind of spin-rotation coupling occasioned by the anisotropic van der Waals interaction, the available rotational states can be mixed together. While j_{12} is a nearly good quantum number, L is not.

For intermediate magnetic moments, the vector diagram is more like Fig. 5(c). Here j_{12} is free to run over many intermediate values, which can be composed of many different orientations of the individual spins $\mathbf{j}_1$ and $\mathbf{j}_2$, which can then interact strongly and anisotropically as the molecules rotates. Here is where the primary channel mixing occurs: at the intermediate-sized magnetic moment.

In summary, not only are the various energy eigenstates of the molecule not all chaotic, in the sense of strongly mixing eigenstates, but moreover, the states that do show this strong mixing are empirically identifiable via trends in their intermediate magnetic moments.

V. CONCLUSION

Every chaotic system, governed by random matrix theory, is chaotic in the same manner. But each system that is only partially chaotic experiences chaos in its own way. Here we have explored the zero-magnetic-field spectrum of a set of lanthanide dimer van der Waals states to locate where their chaos resides. Among the $|JM\rangle = |16 - 16\rangle$ states considered for Dy_2, we find that states belong to one of three realms of qualitatively different chaoticity, loosely correlated to the magnetic moment μ of the state. States with the highest values of μ tend to be nonchaotic and described by the quantum numbers j_{12} and L; states of the lowest μ are mildly chaotic due to mixing of the orientation of the molecular rotation L; and states with intermediate values of μ near the mean are "just right" for chaos, capable of mixing both the spin and rotation states.

This report has dealt only with molecules associated with the spin-stretched atomic states $|jm\rangle = |8 - 8\rangle$ most closely allied with experiment, but many other manifolds of states exist. Future work should be able to find similar systematics in the spectra and establish a zoology of van der Waals lanthanide dimers. More significantly, the results remain to be extended to the case of nonzero magnetic field. One presumes the appearance and pattern of chaos may take different forms when states of different angular momentum J are coupled and the molecules become overall more chaotic [3,19]. In this context it is worth noting that even more exotic states of lanthanide dimers have been proposed, which possess large electric dipole moments as well as large magnetic dipole moments, providing additional opportunities for introducing and probing chaos [30,31].

In the broader sense, these results imply the ability to identify molecular states with qualitatively different manifestations of chaos by virtue of their magnetic moment. This ability can be useful in dynamical studies of these chaotic molecules. For example, having prepared the molecule in a particular state, a sudden quench to a different magnetic field value will project this state onto a host of other energy eigenstates and will initiate dynamics. Knowing what the states are likely to be like, one can imagine different quenches to and from molecules that are either rotationally chaotic, spin chaotic, or both. The richness of the resulting dynamics remains to be contemplated.

ACKNOWLEDGMENTS

We gratefully acknowledge useful discussions with M. Lepers. This material is based upon work supported by the National Science Foundation under Grants No. PHY 1734006 and No. PHY 1806971. L.D.A. acknowledges the financial support of the Czech Science Foundation (Grant No. 18-00918S).

APPENDIX: HAMILTONIAN MATRIX ELEMENTS

The laboratory- and body-frame basis sets are related by a unitary transformation with matrix elements

$$\langle j_{12}\bar{\Omega}; JM|[j'_{12}L']J'M'\rangle = \frac{2}{\sqrt{2(1+\delta_{\bar{\Omega}0})}}(-1)^{M-\bar{\Omega}}\sqrt{2L'+1}\begin{pmatrix} j_{12} & L' & J \\ \bar{\Omega} & 0 & -\bar{\Omega}\end{pmatrix} \times \delta_{j_{12}j'_{12}}\delta_{JJ'}\delta_{MM'}. \quad \text{(A1)}$$

Thus the various pieces of the Hamiltonian can be cast in either basis, as convenient, and easily transformed to the other as necessary.

Bearing in mind the transformations between the basis sets, different parts of the Hamiltonian are easy to write in different bases and transformed to the other as necessary. Thus the interaction terms $H_{\rm BO}$, H_{dd}, and H_{ad} are easily written in the body frame, while T and $H_{\rm B}$ take simple forms in the laboratory frame.

1. Kinetic Energy

The kinetic energy takes the usual form,

$$T = -\frac{\hbar^2}{2m_r}\frac{d^2}{dR^2} + T_{\rm cent}, \tag{A2}$$

where m_r is the reduced mass of the colliding pair, and the centrifugal part is diagonal in the laboratory basis,

$$T_{\rm cent} = -\frac{\hbar^2 L(L+1)}{2m_r R^2}\delta_{j_{12}j'_{12}}\delta_{LL'}\delta_{JJ'}\delta_{MM'}. \tag{A3}$$

2. Born-Oppenheimer Potentials

The Born-Oppenheimer part is determined, in general, from detailed electronic structure calculations. These have been carried out for Dy and Er, but instead we find it convenient to use simpler, analytic forms as a stand-in for these potentials.

The molecular axis is an axis of rotational symmetry for the interactions among the electrons and nuclei that make up the molecule, whereby $\bar{\Omega}$ is a good quantum number and the body-frame basis makes sense. The total spin angular momentum j_{12} need not be a good quantum number, and different values may be somehow coupled together. However, the parity of j_{12} is good: the gerade states have even j_{12} values, and the nongerade states have odd j_{12} values. This Hamiltonian is, moreover, independent of the total rotational state of the molecule and hence independent of J and M.

We simplify diagonal elements of H_{BO} by employing a set of Lennard-Jones potentials,

$$\langle j_{12}\bar{\Omega}; JM|H_{\rm BO}|j_{12}\bar{\Omega}; JM\rangle = \frac{C_{12}(\bar{\Omega}, j_{12})}{R^{12}} - \frac{C_6}{R^6}. \tag{A4}$$

Here each channel as assumed to have the same isotropic van der Waals coefficient C_6, as the anisotropy is dealt with separately. Each diagonal channel may have a different C_{12} coefficient, which may be drawn from a statistical ensemble so that these potentials have random scattering lengths, if desired. However, in the results below, we employ a particular value of C_{12} in all channels. Likewise, it would be possible to generate random matrix elements that couple different values of j_{12}, but we have not done so here. This approach exploits the observation of Ref. [3] that the dominant channel coupling occurs due to the anisotropic van der Waals interaction. For the calculations described below, we use $C_6 = 2274$ a.u. [32] and artificially truncate the potentials at small R using the same value $C_{12} = 1.0 \times 10^{11}$ a.u. in all channels.

3. Dipole-Dipole Interaction

The dipole-dipole interaction is also naturally described in the body frame, where it is diagonal in $\bar{\Omega}$:

$$\langle j_{12}\bar{\Omega}; JM|V_{dd}|j'_{12}\bar{\Omega}'; J'M'\rangle = -\frac{\sqrt{30}(g\mu_B)^2}{R^3}\frac{1+(-1)^{j_{12}+j'_{12}}}{2}\delta_{\bar{\Omega}\bar{\Omega}'}\delta_{JJ'}\delta_{MM'}(-1)^{j_{12}-\bar{\Omega}}j(j+1)(2j+1)\sqrt{(2j_{12}+1)(2j'_{12}+1)}$$
$$\times\begin{Bmatrix} j_{12} & j'_{12} & 2 \\ j & j & 1 \\ j & j & 1 \end{Bmatrix}\begin{pmatrix} j_{12} & 2 & j'_{12} \\ \bar{\Omega} & 0 & -\bar{\Omega}\end{pmatrix}, \tag{A5}$$

where $j = j_1 = j_2$. The coupled spin j_{12} is not conserved by this interaction, but its parity is.

4. Anisotropic Dispersion Interaction

For large R, the atoms also exert anisotropic dispersion forces on each other. These are evaluated in detail in Ref. [25]. The dominant dispersion term is, of course, the isotropic one described above. Second to this, and the only non-negligible correction in this context, is the term given explicitly in the uncoupled, body-frame basis by [25]

$$\langle j_1\omega_1 j_2\omega_2|V_{ad}|j_1\omega_1 j_2\omega_2\rangle = \sqrt{\frac{5}{2}}\frac{C_{6,20}}{R^6}(\langle j_1\omega_2 20|j_1\omega_1\rangle + \langle j_1\omega_2 20|j_2\omega_2\rangle), \tag{A6}$$

where $C_{6,20}$ is a numerical coefficient derived in perturbation theory. Adapting this to the coupled body-frame basis gives the matrix elements

$$\langle j_{12}\bar{\Omega}; JM|V_{ad}|j'_{12}\bar{\Omega}'; J'M'\rangle = \frac{C_{6,20}}{R^6}\frac{1+(-1)^{j_{12}+j'_{12}}}{2}\delta_{\bar{\Omega}\bar{\Omega}'}\delta_{JJ'}\delta_{MM'}(-1)^{2j-\bar{\Omega}}\sqrt{10}\sqrt{(2j+1)(2j_{12}+1)(2j'_{12}+1)}$$
$$\times\begin{Bmatrix} j & j_{12} & j \\ j'_{12} & j & 2 \end{Bmatrix}\begin{pmatrix} j_{12} & 2 & j'_{12} \\ \bar{\Omega} & 0 & -\bar{\Omega}\end{pmatrix}. \tag{A7}$$

Just as for dipoles, $\bar{\Omega}$ is conserved, as is the parity of j_{12}, but j_{12} itself is not.

The constant $C_{6,20}$ in front of this expression is subject to considerable uncertainly in the literature. In general, the strength of the anisotropic dispersion contribution is characterized by diagonalizing the matrix (A7), exclusive of $1/R^6$, and defining ΔC_6 as

the difference between the maximum and minimum eigenvalues. Reported values of this constant include $\Delta C_6 = 5.8$ a.u. [33], $\Delta C_6 = 14$ a.u. [32], $\Delta C_6 = 25$ a.u. [9], and $\Delta C_6 = 174$ a.u. [19]. In the interest of incorporating significant channel mixing in the model, we will use the last value, which corresponds to $C_{6,20} = -44.4$ a.u.

5. Magnetic Field Hamiltonian

The magnetic field acts on the magnetic moments of the atoms separately,

$$H_B = g\mu_B B T_0^1(\mathbf{j}_1) + g\mu_B B T_0^1(\mathbf{j}_2). \tag{A8}$$

Its matrix elements are conveniently written in the coupled laboratory frame as

$$\begin{aligned}\langle [j_{12}L]JM|H_B|[j'_{12}L']J'M'\rangle &= g\mu_B B[(-1)^{j_{12}} + (-1)^{j'_{12}}]\delta_{LL'}\delta_{MM'}(-1)^{J-M+J'+j_{12}+L} \\ &\times \sqrt{j(j+1)(2j+1)(2j_{12}+1)(2j'_{12}+1)(2J+1)(2J'+1)} \\ &\times \begin{Bmatrix} j_{12} & J & L \\ J' & j'_{12} & 1 \end{Bmatrix} \begin{Bmatrix} j & j_{12} & j \\ j'_{12} & j & 1 \end{Bmatrix} \begin{pmatrix} J & 1 & J' \\ -M & 0 & M \end{pmatrix}.\end{aligned} \tag{A9}$$

This interaction is capable of mixing different values of the total angular momentum that differ by 1. j_{12} could also change by 1, except that its parity must be conserved. Therefore this matrix element is diagonal in j_{12}.

[1] A. Frisch *et al.*, Nature **507**, 475 (2014).

[2] K. Baumann, N. Q. Burdick, M. Lu, and B. L. Lev, Phys. Rev. A **89**, 020701(R) (2014).

[3] T. Maier, H. Kadau, M. Schmitt, M. Wenzel, I. Ferrier-Barbut, T. Pfau, A. Frisch, S. Baier, K. Aikawa, L. Chomaz, M. J. Mark, F. Ferlaino, C. Makrides, E. Tiesinga, A. Petrov, and S. Kotochigova, Phys. Rev. X **5**, 041029 (2015).

[4] V. A. Khlebnikov, D. A. Pershin, V. V. Tsyganok, E. T. Davletov, I. S. Cojocaru, E. S. Fedorova, A. A. Buchachenko, and A. V. Akimov, Phys. Rev. Lett. **123**, 213402 (2019).

[5] G. Durastante, C. Politi, M. Sohmen, P. Ilzhöfer, M. J. Mark, M. A. Norcia, and F. Ferlaino, Phys. Rev. A **102**, 033330 (2020).

[6] J. Mur-Petit and R. A. Molina, Phys. Rev. E **92**, 042906 (2015).

[7] K. Roy, B. Chakrabarti, N. D. Chavda, V. K. B. Kota, M. L. Lekala, and G. J. Rampho, Europhys. Lett. **118**, 46003 (2017).

[8] L. D. Augustovičová and J. L. Bohn, Phys. Rev. A **98**, 023419 (2018).

[9] S. Kotochigova and A. Petrov, Phys. Chem. Chem. Phys. **13**, 19165 (2011).

[10] C. B. Connolly, Y. S. Au, S. C. Doret, W. Ketterle, and J. M. Doyle, Phys. Rev. A **81**, 010702(R) (2010).

[11] B. K. Newman, N. Brahms, Y. S. Au, C. Johnson, C. B. Connolly, J. M. Doyle, D. Kleppner, and T. J. Greytak, Phys. Rev. A **83**, 012713 (2011).

[12] J. J. McClelland and J. L. Hanssen, Phys. Rev. Lett. **96**, 143005 (2006).

[13] D. Sukachev, A. Sokolov, K. Chebakov, A. Akimov, S. Kanorsky, N. Kolachevsky, and V. Sorokin, Phys. Rev. A **82**, 011405(R) (2010).

[14] S. H. Youn, M. Lu, U. Ray, and B. L. Lev, Phys. Rev. A **82**, 043425 (2010).

[15] A. Frisch, K. Aikawa, M. Mark, A. Rietzler, J. Schindler, E. Zupanic, R. Grimm, and F. Ferlaino, Phys. Rev. A **85**, 051401(R) (2012).

[16] A. Trautmann, P. Ilzhofer, G. Durastante, C. Politi, M. Sohmen, M. J. Mark, and F. Ferlaino, Phys. Rev. Lett. **121**, 213601 (2018).

[17] T. Maier, I. Ferrier-Barbut, H. Kadau, M. Schmitt, M. Wenzel, C. Wink, T. Pfau, K. Jachymski, and P. S. Julienne, Phys. Rev. A **92**, 060702(R) (2015).

[18] E. Lucioni, L. Tanzi, A. Fregosi, J. Catani, S. Gozzini, M. Inguscio, A. Fioretti, C. Gabbanini, and G. Modugno, Phys. Rev. A **97**, 060701(R) (2018).

[19] C. Makrides, M. Li, E. Tiesinga, and S. Kotochigova, Sci. Adv. **4**, eapp8308 (2018).

[20] V. K. B. Kota, *Embedded Random Matrix Ensembles in Quantum Physics*, Lecture Notes in Physics Vol. 884 (Springer, Heidelberg, 2014).

[21] L. D'Alessio, Y. Kafri, A. Polkovnikov, and M. Rigol, Adv. Phys. **65**, 239 (2016).

[22] A. Frisch, M. Mark, K. Aikawa, S. Baier, R. Grimm, A. Petrov, S. Kotochigova, G. Quéméner, M. Lepers, O. Dulieu, and F. Ferlaino, Phys. Rev. Lett. **115**, 203201 (2015).

[23] R. V. Krems, G. C. Groenenboom, and A. Dalgarno, J. Phys. Chem. A **108**, 8941 (2004).

[24] G. C. Groenenboom, X. Chu, and R. V. Krems, J. Chem. Phys. **126**, 204306 (2007).

[25] M. Lepers and O. Dulieu, in *Cold Chemistry: Molecular Scattering and Reactivity Near Absolute Zero*, edited by O. Dulieu and A. Osterwalder, Theoretical and Computational Chemistry Series No. 11 (Royal Society of Chemistry, 2018).

[26] C. C. Marston and G. G. Balint-Kurti, J. Chem. Phys. **91**, 3571 (1989).

[27] J. Brown and A. Carrington, *Rotational Spectroscopy of Diatomic Molecules* (Cambridge University Press, Cambridge, England, 2013).

[28] Note that this mean value is given by the average of the diagonal elements of the operator $\mathcal{M}$, that is, $(1/N)\sum_{i=1}^{N}\langle i|\mathcal{M}|i\rangle = (1/N)\mathrm{Tr}(\mathcal{M})$, and the trace of the operator is basis independent.

[29] R. N. Zare, *Angular Momentum: Understanding Spatial Aspects in Chemistry and Physics* (Wiley, New York, 1986).

[30] H. Li, G. Quéméner, J.-F. Wyart, O. Dulieu, and M. Lepers, Phys. Rev. A **100**, 042711 (2019).

[31] M. Lepers, H. Li, J.-F. Wyart, G. Quéméner, and O. Dulieu, Phys. Rev. Lett. **121**, 063201 (2018).

[32] M. Lepers (private communication).

[33] H. Li, J.-F. Wyart, O. Dulieu, S. Nascimbène, and M. Lepers, J. Phys. B **50**, 014005 (2017).